Chapter 4
Third Section: Design of a dimeric-nanobody specific for $A\beta_{42}$ oligomers: the Dimeric-DesAb-O

1. Dimeric-DesAb-O design

The rationale behind the engineering of DesAb-O was to design a dimeric sdAb able to bind $A\beta_{42}$ oligomers with a higher binding avidity and specificity. It is conceivable that the dimer may be capable of binding to multiple exposed binding sites within the oligomeric structure, rather than binding to a single exposed monomeric binding site. This could result in an enhanced binding avidity and specificity for oligomeric structures, rather than a stronger affinity. However, it is challenging to distinguish between an increased avidity or affinity. Consequently, we evaluated them as a whole, rather than analysing them individually.

To obtain a dimeric structure of this sdAb, a flexible linker $(GGGGS)_3$, consisting of a repetition of glycine (Gly) and serine (Ser) residues over a length of 15 amino acids (Huston *et al*. 1988), was attached to the C-terminus of the first monomer and the N- terminus of the second monomer, cleaved from its His-tagged region, as reported in Figure 4.1. In particular, the N-terminus of DesAb-O presents a solvent-exposed loop region composed of approximately 34 amino acids, mainly composed of Ser and Gly, as the flexible linker described above, as well as threonine (Thr), proline (Pro), aspartic acid (Asp), lysine (Lys), glutamine (Gln) and alanine (Ala), which have been suggested as preferred linker elements by Argos (Argos 1990; Chen, Zaro and Shen 2013). Together, these features represent a good composition for a *partial natural linker*, composed by the flexible $(GGGGS)_3$ linker and the loop region of the second monomer, for a total length of 39 amino acids (Figure 4.1). The length of the linker guarantees a wide range of movement of both domains and the possibility of binding antigen sites

Liliana Napolitano, liliana98.napolitano@gmail.com, 0009-0004-3087-286X

Referee List (DOI 10.36253/fup_referee_list)
FUP Best Practice in Scholarly Publishing (DOI 10.36253/fup_best_practice)

Liliana Napolitano, Third Section*: Design of a dimeric-nanobody specific for $A\beta_{42}$ oligomers: the Dimeric-DesAb-O*, © Author(s), CC BY 4.0, DOI 10.36253/979-12-215-0993-9.06, in Liliana Napolitano, *A multidisciplinary approach for the early diagnosis of Alzheimer's disease and potential therapeutic applications*, pp. 95-115, 2026, published by Firenze University Press, ISBN 979-12-215-0993-9, DOI 10.36253/979-12-215-0993-9

Book References DOI 10.36253/979-12-215-0993-9.references

distance between them (Chen, Zaro and Shen 2013; Yusakul *et al*. 2016) The gene sequence was modified using software SnapGene (www.snapgene.com).

2. Structural characterization of the Dimeric-DesAb-O

The Dimeric-DesAb-O was expressed in *E. coli* and purified, as detailed in Figure 4.2. Thereafter, the secondary structure, molecular weight and thermal stability were characterised by CD and ESI-MS, as reported in Figure 4.3. CD spectroscopy demonstrated that the dimeric structure of DesAb-O exhibits a predominant β-sheet secondary structure, similar to that observed for the monomer (Figure 4.3 A). To provide a more accurate interpretation of the CD spectra of these sdAbs, the BestSel software (v1.3.230210; Micsonai *et al*. 2018) was employed (Table 4.1).

BestSel analysis revealed an increased proportion of antiparallel β-sheet secondary structure for the Dimeric-DesAb-O compared to DesAb-O (61% and 57%, respectively). Notably, DesAb-O comprises 7% parallel β-sheet, an element that is entirely absent from the dimeric structure profile. Conversely, the dimeric sdAb exhibits a 3% α-helix, likely attributable to the presence of the linker, which is absent in the BestSel results for DesAb- O, as reported in Table 4.1.

To evaluate the molecular weight of the engineered DesAb-O, we employed the use of ESI-MS, as represented in Figure 4.3 B. From the ESI-MS spectrum, the mass of the Dimeric-DesAb-O construct was determined to be 34.270 Da. The experimental value was found to be in complete agreement with the theoretical measurements obtained with with ExPASy ProtParam (Gill and Von Hippel 1989) (34.269 Da), which were used to derive the molecular weight.

To assess whether the new dimeric construct had similar structural stability as the monomeric DesAb-O, we performed a thermal denaturation experiment to determine the temperature of half-denaturation (*Tm*) (Figure 4.3 C). CD spectra were recorded between 20 °C and 90 °C to monitor the thermal unfolding of the protein (Figure 4.3 C). The sdAbs concentration was 6 μM in PBS pH 7.4. The molar residue ellipticity per residue ($[\theta]_{res}$) at a 210 nm was extracted from each CD spectrum and plotted as a function of temperature (Figure 4.3 D). The resulting thermal denaturation curves were fitted with a two-state model and normalised to fraction folded (%) values. The sdAbs share very close thermal denaturation points as the Dimeric-DesAb-O had a *Tm* of 72.7 °C, whereas the value for DesAb-O was 74.6 °C (Figure 4.3 D). This structural characterisation showed how the engineering of DesAb-O and the addition of a flexible linker resulted in a stable dimeric sdAb that shared the secondary structure and a *Tm* close to the monomeric sdAb

3. The Dimeric-DesAb-O slows down $A\beta_{42}$ aggregation in a dose-dependent manner

To assess the ability of the Dimeric-DesAb-O to interfere on the $A\beta_{42}$ aggregation process, we performed ThT assays on solutions containing 1 μM

monomeric $A\beta_{42}$ in the presence of decreasing $A\beta_{42}$ monomeric:Dimeric-DesAb-O molar ratios (1:1, 1:0,5, 1:0,25, 1:0,125), as reported in Figure 4.4 A. Interestingly, the Dimeric-DesAb-O massively reduced the $A\beta_{42}$ aggregation process at the 1:1 molar ratio, increasing the aggregation half-time (t_{50}) approximately 2-fold compared to $A\beta_{42}$ alone (3.2 ± 1.1 h and 1.5 ± 0.4, respectively). Furthermore, the t_{50} of the co-incubated $A\beta_{42}$ and Dimeric-DesAb-O samples decreased proportionally with decreasing Dimeric-DesAb-O concentration (2 ± 0.4 h for 1:0.5; 1.8 ± 0.3 for 1:0.25; 1.7 ± 0.3 h for 1:0.125; $A\beta_{42}$ monomeric:Dimeric-DesAb-O respectively), demonstrating the remarkable ability of the Dimeric-DesAb-O to interfere with the $A\beta_{42}$ aggregation process even at low concentrations (Figure 4.4 A).

To evaluate the improvement of the dimeric sdAb with respect to DesAb-O, we tested increasing molar ratios of $A\beta_{42}$ monomeric:DesAb-O (1:1, 1:2) as represented in Figure 4.4 B. The aggregation profile obtained with increasing DesAb-O molar ratios slightly increased the t_{50} (1.8 ± 0,6 h for 1:2, 1.7 ± 0.4 h for 1:1, 1.5 ± 0.4 h $A\beta_{42}$ monomeric:DesAb-O respectively) slowing down the $A\beta_{42}$ aggregation process. Despite this interference, DesAb-O did not slow the aggregation process to the same extent as the Dimeric-DesAb- O, increasing the t_{50} only 1.3-fold at 1:2 $A\beta_{42}$ monomer:sdAb molar ratio. Notably, the dimeric form of DesAb-O exhibited a comparable inhibitory effect at a significantly lower molar ratio of 1:0.25 (by 1.8 ± 0.5 h) indicating a substantially greater potency in interfering with the aggregation process of the $A\beta_{42}$.

4. Dimeric-DesAb-O has improved specificity of binding for $A\beta_{42}$ oligomers

With the aim of investigating the specificity and selectivity of the Dimeric-DesAb-O for $A\beta_{42}$ oligomeric conformers, we performed a Real-Time Based ELISA assay using DesAb-O as control. To do so, we prepared solutions of 1 μM $A\beta_{42}$,and we monitored the aggregation of $A\beta_{42}$ by ThT (Figure 4.4 C). The aggregation reaction was stopped at different timepoints (0, 0.5, 1, 2, 22 h) to collect $A\beta_{42}$ samples to adsorb in an ELISA plate overnight. The following day, 1 μM DesAb-O or 1 μM Dimeric-DesAb-O were used as primary antibodies. The absorbance signals were all compared against the timepoint 0 h. Our experiments showed that after 0.5 h, the Dimeric-DesAb-O slightly increased the absorbance signal probably due to the initial formation of low molecular weight aggregates, exhibiting a statistically difference with DesAb-O at the same time (Figure 4.4 D). As the time-course continues, our experiments revealed a significant increase in absorbance signal for both sdAbs, especially after 1 and 2 h from the begging of the aggregation, approximately close to the half-time of aggregation as determined by ThT (Figure 4.4 C,D), where oligomers are at their maximum amount. At these timepoints, the Dimeric-DesAb-O exhibited the highest absorbance being approximately 2-fold higher than that initial aggregation time point, showing a significant difference compared to DesAb-O at the same time. After 20 hours of aggregation, the Dimeric- DesAb-O still showed an absorbance

approximately 1.3-fold higher than time 0, indicating the binding to $A\beta_{42}$ species, while DesAb-O returned to similar absorbance levels as the initial ones, as previously reported (Aprile *et al*. 2020). In order to understand whether the dimeric form of DesAb-O was recognising $A\beta_{42}$ oligomers or $A\beta_{42}$ fibrillar conformers, we used $A\beta_{42}$ fibrils obtained after 4 days of incubation at 37 °C as a control, as represented in Figure 4.4 D. Interestingly, neither sdAbs recognised these $A\beta_{42}$ fibrils, resulting in an absorbance signal well below timepoint 0. From this evidence, we can assess that the Dimeric-DesAb-O is able to recognise $A\beta_{42}$ oligomers at very low concentrations, with high specificity and affinity, representing a successful improvement of the previous outstanding DesAb-O specificity for $A\beta_{42}$ oligomers.

5. Dimeric-DesAb-O induces morphological and structural changes in $A\beta_{42}$ fibrils

To further investigate the impact of the Dimeric-DesAb-O on the $A\beta_{42}$ aggregation, we analysed the structural and morphological changes induced in $A\beta_{42}$ fibrils upon incubation with this dimeric sdAb. To do so, 5 μM $A\beta_{42}$ samples obtained in the absence or in the presence of equimolar concentration of DesAb-O or Dimeric-DesAb-O at the end of a ThT aggregation assay were visualized by taking advantage of Transmission Electron Microscopy (TEM) (Figure 4.5 A). From our analysis, the $A\beta_{42}$ fibrillar structures obtained in the absence of sdAbs showed a dense network of connections (Figure 4.5 A, first column), presenting a diameter of approximately 11.5 ± 0.1 nm, as represented in Figure 4.5 B. On the contrary, $A\beta_{42}$ fibrils obtained from co- incubation with DesAb-O showed a reduced ability to form connections and a tendency to fracture, as indicated by the symbol * (Figure 4.5 A, second column). Furthermore, these $A\beta_{42}$ fibrils exhibited a reduced diameter width with respect to $A\beta_{42}$ fibrils obtained in the absence of sdAbs, averaging 10 ± 1 nm (Figure 4.5 B). Interestingly, a striking change in the morphology of $A\beta_{42}$ fibrils occurs when monomeric $A\beta_{42}$ is co-incubated with the Dimeric-DesAb-O. In fact, fibrils have shown jagged appearance with the presence of globular structures on their surface (Figure 4.5 A, third column). In addition, from TEM images background we can observe the presence of electrodense short fragments suggesting that fibrils may be breaking or degrading due to increased structural weakness. Furthermore, these $A\beta_{42}$ fibrils exhibited a further reduction in diameter compared to those formed in the presence of DesAb-O resulting exceptionally thin, with an average (7.4 ± 0.6 nm), and suggesting a more potent inhibitory effect of the dimeric sdAb on fibril assembly (Figure 4.5 B).

In order to investigate the increased $A\beta_{42}$ fibrils fragility induced by the sdAbs co- incubation with $A\beta_{42}$ monomer in ThT aggregation assays, we performed a Dot Blot assay. Briefly, samples were collected at the end of a ThT experiment and centrifuged at max speed (~17,000*g*) for 30 min on a benchtop

centrifuge to separate the soluble and insoluble aggregates, as previously reported (Vadukul *et al.* 2023). Prior to centrifugation, an aliquot of each sample was reserved and considered as the total protein amount. To analyze the distribution of $A\beta_{42}$ and sdAbs, samples were spotted onto nitrocellulose membrane and incubated with 6E10 Abs for $A\beta_{42}$ detection or anti-6X His-tag Abs for sdAbs detection. The signal intensity in the supernatant was normalized to the total protein content of the corresponding sample. Quantifications of $A\beta_{42}$ fibrils and sdAbs deposited into the pellet are represented in Figure 4.6.

Our results showed that samples of $A\beta_{42}$ fibrils obtained in the absence of sdAbs showed a low presence in the supernatant (14 ± 3%) and high amount (88 ± 5%) in the pellet, respectively (Figure 4.7 A). This might indicate a high strength and robustness of the fibrils, which do not tend to break or resuspend in the supernatant. Conversely, samples obtained in the presence of DesAb-O and Dimeric-DesAb-O displayed an increased occurrence of fibrillar material in the supernatant (22 ± 2% and 36 ± 2%; respectively) and only partial deposition in the pellet (79 ± 5% and 68 ± 5%; respectively), as represented in Figure 4.7 A. This suggests an increase in fibril fragility and a heightened tendency for fragmentation. Moreover, the presence of smaller fragments in the supernatant, likely due to their reduced ability to sediment effectively during centrifugation, further supports this observation.

This fragmentation also explains the presence of material in the background of the TEM images, as noted earlier. Even more surprisingly, our results showed that DesAb-O was predominantly adhered to the $A\beta_{42}$ fibrils deposited in the pellet (17% ± 2% and 84% ± 4%; for supernatant and pellet respectively), whereas in contrast, the Dimeric-DesAb-O was more adhered to the fragments found in the supernatant of the samples (58% ± 9% and 50% ± 3%, for supernatant and pellet respectively) (Figure 4.7 B). The observation that $A\beta_{42}$ forms thinner and more fragile fibrils in the presence of the Dimeric-DesAb-O, with a greater occurrence of this sdAb in the fragments, suggests that the dimeric form of DesAb-O may interfere with $A\beta_{42}$ assembly, promoting its fragmentation. Furthermore, the dimeric sdAb may bind to $A\beta_{42}$ oligomers, stabilizing them and preventing their aggregation.

We further investigate the ability of sdAbs to modify the structure of $A\beta_{42}$ fibrils. Thus, we carried out a proteinase K (PK) digestion assay (Figure 4.7 C) to determine whether sdAbs co-incubation could influence the PK digestion sensitivity due to the generation of structural modifications in $A\beta_{42}$ fibrils. Briefly, fibrils were collected from the co-incubation sample with sdAbs at the end of aggregation by centrifugation at max speed (~17,000*g*) for 1 h, resuspended in PBS and treated with 0, 10, 25, 50 μg/mL PK for 30 mins. Samples were then incubated at 95 °C for 5 min to stop the enzymatic reaction and loaded on SDS-PAGE for a Western blotting analysis as previously reported (Vadukul *et al*. 2023). Bands intensity at each concentration were normalized on the 0 μg/mL correspondent band. Our results showed that $A\beta_{42}$ fibrils obtained in the presence of DesAb-O displayed an increased resistance to PK digestion at low

PK concentrations (10 μg/mL) while samples obtained in the absence of sdAbs and in the presence of the Dimeric-DesAb-O followed a similar trend, shared by samples co-incubated with DesAb- O at increased PK concentrations, as represented in Figure 4.7 E.

These results demonstrate that the co-incubation with sdAbs during the $A\beta_{42}$aggregation process induces important and fundamental changes in the structure of $A\beta_{42}$ fibrils. Furthermore, the co-incubation with the Dimeric-DesAb-O, as evidenced by dot blot and TEM microscopy, resulted in impressive changes, leading to a reduction in fiber diameter, increased fragility and a greater tendency to form stabilized aggregate structures. Taken together, this evidence indicates the strong tendency of this dimeric sdAb to interfere with $A\beta_{42}$ aggregation.

6. Characterisation of $A\beta_{42}$ aggregates with ThT assay, dot blot assay and STED microscopy

With the aim of obtaining transient $A\beta_{42}$ aggregates for cell biology experiments, we used the $A\beta_{42}$ synthetic peptide. Initially, we characterised the $A\beta_{42}$ aggregation by ThT assay, confirming that the synthetic $A\beta_{42}$ peptide aggregation occurs in a manner comparable to the recombinant peptide. Precisely, samples of synthetic $A\beta_{42}$ monomers at 10 µM was mixed with 25µM ThT, incubated at 37 °C and ThT fluorescence was monitored at 482 nm over a span of 24 h. The progressive increase of the ThT fluorescent signal provides insight into β-sheets formation. Concomitantly, we collected aliquots of the reaction solution at different timepoints (0, 2, 4, 8 and 24 h) in order to characterise the reactive properties and the morphology of the species formed during the aggregation process (Figure 4.8). We took advantage of dot blot assay and super resolution STED microscopy coupled with conformation-sensitives Abs able to distinguish specific $A\beta_{42}$ aggregate conformations. In particular, we used the anti-ADDLs 19.3 Ab (Savage *et al*. 2014) and the anti-amyloid fibrils OC Ab (Kayed *et al.* 2007). As controls, we used the 6E10 Ab, which binds to the N-terminus of $A\beta_{42}$ peptides without distinguishing between different conformations. At 0 h we found a higher ThT signal compared to the buffer-only samples, called control in Figure 4.8 A, with only a minimal positivity for 19.3 Ab and none for OC Ab in the dot blot assay and STED images (Figure 4.8 B,C,D,E). After 2 h of incubation, we observed an increase in ThT fluorescence, indicating the formation of aggregated species (Figure 4.8 A), that appeared positive for 19.3 Ab and to a lesser extent for OC Ab (Figure 4.8 C,D). At T2, the ThT fluorescent signal further increased (Figure 4.8 A), as well as the positivity for 19.3 Ab and only a minor signal for OC Ab (Figure 4.8 C,D). After 8 h, we found the exponential phase of the sigmoidal curve and a sharp increase in ThT fluorescent signal (Figure 4.8 A). Concurrently, strong positivity with 19.3 Ab and the presence of numerous small, globular species in STED images (Figure 4.8 C,E) indicated the highest concentration of oligomers. We also noticed a positivity for OC Ab (Figure 4.8 D,E), indicating the formation of few fibrillary species. At the end of the

aggregation reaction, the ThT curve reached a plateau (Figure 4.8 A), suggesting the presence of $A\beta_{42}$ fibrils and the end of new aggregate formation. Dot blot assays and STED images showed positivity for OC Ab together with the presence of fibrillary elongated species and only a minor presence of oligomers (Figure 4.8 D,E). As control, 6E10 Ab exhibited positivity for each type of species (Figure 4.8 B,E), indicating the proper loading and the progressive maturation of $A\beta_{42}$ fibrils. Overall, STED imaging and Dot blot analyses reveals that after 8 hours of incubation, the $A\beta_{42}$ solution becomes heterogeneous, comprising a mixture of oligomers, pre-fibrillar aggregates, and low molecular weight fibrils.

7. $A\beta_{42}$ oligomeric species obtained after 8 hours of incubation exhibit high toxicity

Then, we investigated the toxicity of the various $A\beta_{42}$ aggregates generated during the $A\beta_{42}$ aggregation process, taking advantage of the MTT reduction test. In this experiment, $A\beta_{42}$ species collected at different timepoints (0, 2, 4, 8 and 24 h) were added to the extracellular medium of SH-SY5Y cells for 24 h. Our findings revealed that $A\beta_{42}$ species formed at the beginning of the aggregation process (0 h), mostly composed of the monomeric form, did not significantly reduce cell mitochondrial activity (16 ± 6%) as compared to untreated cells, taken as 100 % (Figure 4.9 A). In contrast, starting from 2 h of aggregation we observed a progressive reduction of cell viability (34 ± 4%) which became significant after 4 h (50 ± 2%) and reached its peak after 8 h (58 ± 3%), in which the solution mostly consists of oligomeric species. Finally, after 24 h, we observed a minor toxicity with respect to the timepoints collected after 4 and 8 h, even if $A\beta_{42}$ conformers still generated a significant reduction of cell viability (41 ± 4%), probably due to the presence of residual $A\beta_{42}$ oligomers and $A\beta_{42}$ fibrils (Figure 4.9 A). These findings suggest that after 8 h of incubation, we have the highest amount of $A\beta_{42}$ oligomers due to the half-time of aggregation as determined by ThT and evidenced by dot blot and STED images. For this reason, $A\beta_{42}$ transient oligomers obtained after 8 h of aggregation performed the highest toxicity.

Therefore, to investigate more into their ability to induce toxicity, we conducted a dose-dependent MTT assay (Figure 4.9 B). Increasing concentrations (ranging from 0.5 pM to 1 μM) of the aggregates formed after 8 h of aggregation were added to the extracellular medium of SH-SY5Y cells for 24 h. Figure 4.9 B illustrates that oligomers caused significant mitochondrial dysfunction only at 0.5 and 1 μM (reduction of 33 ± 3% and 51 ± 2%, respectively).

8. The Dimeric-DesAb-O detects $A\beta_{42}$ oligomers interacting with cellular membranes and internalized into the cytoplasm

For cell biology experiments, we used the $A\beta_{42}$ synthetic peptide from which we characterised the $A\beta_{42}$ aggregation by ThT assay, confirming that the synthetic $A\beta_{42}$ peptide aggregation occurs in a manner comparable to the

recombinant peptide. Furthermore, we characterized aggregates obtained at different timepoints, taking advantage of Dot Blot assay and STED microscopy (Figure 4.8) and we characterized their toxicity by MTT assay (Figure 4.9). Given the great ability of DesAb-O to selectively detect $A\beta_{42}$ in cultured cells as previously reported in Bigi *et al*. 2024b, we investigate the capability of the Dimeric-DesAb-O to detect $A\beta_{42}$ oligomers in cells model and whether the engineering had resulted in an increased ability DesAb-O to detect $A\beta_{42}$ oligomeric conformers. Briefly, human neuroblastoma SH-SY5Y cells were exposed to 0.5 μM $A\beta_{42}$ oligomers for 1 h. Plasma membrane (red channel) and $A\beta_{42}$ aggregates (green channel) were counterstained and analysed by confocal microscopy, as previously reported (Bigi *et al*. 2024b). Two different concentrations, 3 μM and 1 μM, were tested for DesAb-O and the Dimeric-DesAb-O as primary antibodies. 6E10 Ab were used as control. Our results showed that at 3 μM both sdAbs highly recognize $A\beta_{42}$ oligomers interacting with neuronal membranes and internalized into the cells (Figure 4.10 A), showing an increase of the green fluorescent signal by 172 ± 13% and 205 ± 18%, for DesAb-O and its dimeric form respectively, with respect to the untreated cells, taken as 100% (Figure 4.10 B). On the contrary, at 1 μM, DesAb-O did not recognize $A\beta_{42}$ oligomers in a statistically significant manner, increasing the green fluorescent signal by 140 ± 17%, while the Dimeric-DesAb-O was still able to recognize $A\beta_{42}$ oligomeric conformers inducing an increase of the green signal by 173 ± 14% (Figure 4.10 B). Furthermore, a heterogeneous aggregate solution including high molecular weight aggregates and small fibrils as previously characterized was used for the cell experiments in this project (Figure 4.10 A). The sdAbs were only able to recognise the oligomeric species with respect to high molecular weight structures, which were recognised by 6E10 Ab (Figure 4.10 A) representing further evidence of their specificity for $A\beta_{42}$ oligomers. Overall, in our experimental conditions, the Dimeric-DesAb-O selectively recognized toxic $A\beta_{42}$ oligomers interacting with cellular membranes even at lower concentrations than DesAb-O, showing a higher sensitivity than the monomeric sdAb and suggesting a very promising potential for the detection of harmful $A\beta_{42}$ species in biological fluids.

9. The Dimeric-DesAb-O inhibits the interaction of $A\beta_{42}$ oligomers with neuronal membranes preventing $A\beta_{42}$-induced neurotoxicity

We then evaluated whether the Dimeric-DesAb-O was able to capture $A\beta_{42}$ oligomers, preventing their interaction with neuronal membranes and the following detrimental effects. With this aim, $A\beta_{42}$ oligomers at 0.5 μM were pre-incubated for 1 h with DesAb- O and the Dimeric-DesAb-O at increasing molar ratios between $A\beta_{42}$ oligomers and sdAbs (1:0.1, 1:0.25, 1:0.5, 1:1, 1:2, 1:3), and these solutions were added to the cell culture medium of SH-SY5Y cells for 15 mins, as previously reported (Bigi *et al*. 2024b). To detect only the oligomers bound to the cell surface, the cellular membrane was not permeabilized at this

stage, thus preventing Ab internalization. The binding affinity of the aggregates for cellular membranes was assessed by confocal microscopy using the 6E10 Ab as a probe. $A\beta_{42}$ oligomers showed to be colocalized with cellular membranes in the absence of pre-incubation with sdAb (Figure 4.11 A) as previously reported (Schengrud 2010; Evangelist *et al*. 2013; Bigi *et al*. 2020; Bigi *et al*. 2024b). Following the pre-incubation with sdAb, the interaction between $A\beta_{42}$ oligomers and the neuronal membranes showed to be significantly reduced. In particular, Dimeric-DesAb-O massively reduce this interaction up to 1:0.1 $A\beta_{42}$ oligomers:sdAb molar ratio (by 810 ± 63%), while DesAb-O and was found to prevent the interaction of the oligomers with the membrane up to 1:0.5 $A\beta_{42}$ oligomers:sdAb molar ratio (by 896 ± 62%) (Figure 4.11 B). These results again suggest the increased avidity of the Dimeric-DesAb-O with respect to DesAb-O for $A\beta_{42}$ oligomers, representing another evidence of the successful engineering of the monomeric sdAb.

10. The Dimeric-DesAb-O prevent from the dysregulation of cytosolic Ca^{2+} homeostasis and the mitochondrial dysfunction induced by $A\beta_{42}$ oligomers

We then evaluated the ability of the Dimeric-DesAb-O to prevent the detrimental effects induced by $A\beta_{42}$ oligomers, such as the increase of intracellular Ca^{2+} levels and the mitochondrial dysfunction. Firstly, we monitored the disruption of cytosolic Ca^{2+} homeostasis, an early upstream event induced by extracellular $A\beta_{42}$, both in cultured neurons and in relevant mouse AD model, in which Ca^{2+} ions flow from the extracellular space into the cytosol (Bigi *et al*. 2023; Fani *et al*. 2022; Demuro *et al*. 2005; Cascella *et al*. 2021). Briefly, SH-SY5Y cells were treated for 15 min with increasing $A\beta_{42}$ oligomers:sdAbs molar ratio, following or not 1 h of pre-incubation. sdAbs were tested alone as controls. Our results showed that $A\beta_{42}$ oligomers caused an extensive Ca^{2+} influx (by 280 ± 2%) relative to untreated cells taken as 100% (Figure 4.12 A,B). Following 1 h of pre-incubation, the Dimeric-DesAb-O markedly reduced the intracellular free Ca^{2+} levels up to 1:0.1 $A\beta_{42}$ oligomers:Dimeric-DesAb-O molar ratio (by 179 ± 3%) showing a higher protective effect compared to DesAb-O that prevents the Ca^{2+} intracellular increase up to 1:0.25 $A\beta_{42}$ oligomers:DesAb-O molar ratio (by 209 ± 5%), as visualized in Figure 4.12 A and quantified in Figure 4.12 B. Of note, both sdAbs does not affect neuronal viability when added alone to the cell medium. From this evidence, the Dimeric-DesAb-O showed an increased protective effect compared to DesAb-O and representing a successful engineering of the initial sdAb.

The protective effect of the Dimeric-DesAb-O was also evaluated by analyzing the mitochondrial status of cultured cells treated with $A\beta_{42}$ oligomers by MTT reduction test (Figure 4.12 C). $A\beta_{42}$ oligomeric species at 0.5 μM were incubated in the absence or presence of increasing $A\beta_{42}$ oligomers:sdAbs molar ratios (1:0.1, 1:0.25, 1:0.5, 1:1, 1:2, 1:3) for 1 h, and then these solutions were

added to the culture medium of SH-SY5Y cells for 24 h. Our results showed that $A\beta_{42}$ oligomers significantly reduced (by 35 ± 2%) the mitochondrial activity of SH-SY5Y cells as compared to untreated cells, taken as 100%, as previously shown (Evangelisti *et al*. 2016; Cascella *et al*. 2017; Bigi *et al*. 2020; Bigi *et al*. 2024b) (Figure 4.12 C). When $A\beta_{42}$ oligomers were pre- incubated for 1 h with decreasing molar ratios of Dimeric-DesAb-O, we observed a significant recover of the mitochondrial functionality up to 1:0.5 $A\beta_{42}$ oligomers:Dimeric- DesAb-O molar ratios (by 24 ± 2%) and reaching its maximum restore at 1:2 $A\beta_{42}$ oligomers:Dimeric-DesAb-O molar ratio (by 19 ± 3%), whereas DesAb-O was able to prevent the mitochondrial impairment only at 1:3 $A\beta_{42}$ oligomers:DesAb-O molar ratio (by 22 ± 1%). At 1:3 molar ratio, we can observe a slightly decreased ability of the Dimeric-DesAb-O to prevent the mitochondrial dysfunction induced by $A\beta_{42}$ oligomers, with respect to the 1:2 molar ratio (by 22 ± 1% and 19 ± 3%, respectively) that it is not observed in other experiments, as reported in Figure 4.12 C. This behavior could be justified by the concentration of the sdAb and the treatment length. Indeed, it is likely that the high concentration of the Dimeric-DesAb-O could lead to increasing interactions between sdAbs domains and the following release of the $A\beta_{42}$ oligomers. Nevertheless, the dimeric structure of DesAb-O still significantly prevents the mitochondrial dysfunction sharing a similar action with DesAb-O at the same molar ratio (Figure 4.12 C).

Considering these results together, we can confirm the increased ability of the Dimeric-DesAb-O to prevent $A\beta_{42}$ oligomers-induced toxicity, representing a promising tool for a future application in AD treatment.

11. The Dimeric-DesAb-O prevents toxic effects induced by the CSFs of AD patients

Considering the encouraging data obtained with the Dimeric-DesAb-O both *in vitro* and in cultured cells and given the previously reported ability of DesAb-O to selectively detect $A\beta_{42}$ oligomers in cultured cells exposed to CSFs of AD patients (Bigi *et al*. 2024b), we performed a proof-of concept experiment on a small set of clinical samples of CSF (n = 4 from AD and from controls subjects). We aimed to evaluate whether the Dimeric-DesAb-O was able to neutralize the cytotoxicity induced by $A\beta_{42}$ oligomeric species present in CSFs derived from AD patients and whether the engineering resulted in improved performance of DesAb-O (Figure 4.13 A,B). Thus, we monitored the dysregulation of cytosolic Ca^{2+} homeostasis in SH-SY5Y treated for 5 h with the CSFs from AD patients and control subjects diluted 1:1 with the cell culture medium, following or not a 1 h pre-incubation with 3 μM or 1 μM sdAbs, as previously reported (Bigi *et al*. 2024b). The CSFs of AD patients significantly increased the intracellular Ca^{2+} concentration (by 190 ± 7%) relative to untreated cells (Figure 4.13 A,B), while the CSFs of control subjects only slightly increased the intracellular Ca^{2+} free levels (by 140 ± 5%). After 1 h of pre-incubation with 3 μM both DesAb-O and

Dimeric-DesAb-O completely reduced the Ca^{2+} dyshomeostasis induced by CSFs derived from AD patients (by 93 ± 3% and 84 ± 5%, respectively) and CSFs from control-subjects (by 96 ± 5% and 95 ± 6%, respectively) both showing a massive protective effect, as represented in Figure 4.13 B. However, decreasing the sdAbs concentration to 1 μM, we observed a reduced ability of DesAb-O to prevent the cytotoxic effects induced by AD CSFs (by 150 ± 6%) whereas the Dimeric-DesAb-O continued to abolish the Ca^{2+} dyshomeostasis induced by these biological fluids derived from AD patients (by 99 ± 5%) (Figure 4.13 B). Moreover, at 1 μM both sdAbs showed a total preservation of the Ca^{2+} dyshomeostasis in cells treated with CSFs derived from control- subjects (by 102 ± 6% and 84 ± 5% for DesAb-O and Dimeric-DesAb-O, respectively) (Figure 4.13 B).

Taken together, these data demonstrate the ability of the Dimeric-DesAb-O to selectively detect and neutralize toxic species present in the CSFs of AD patients. Our data also indicate that the engineering of DesAb-O has led to the production of a promising tool for future potential application in the diagnosis, therapy and prognosis of AD, improving on the previous excellent ability of DesAb-O.

12. Chapter 4: figures and tables

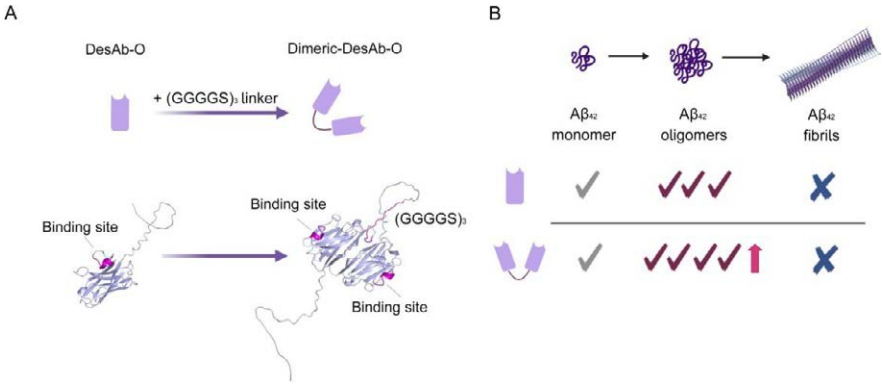

Figure 4.1 - Dimeric-DesAb-O design. A Schematic representation of the ingeneration of DesAb-O (left) to obtain the Dimeric-DesAb-O (right). A) Representative binding sites and loop region highlighted in bright purple. 3D reconstruction was obtained Alphaphold Colab 2. B) Schematic representation of the aim of the study. We designed a dimeric structure of DesAb-O to obtain an enhanced specificity and affinity for $A\beta_{42}$ oligomers, while avoiding increased binding to $A\beta_{42}$ monomers or fibrils.

	DesAb-O (%)	Dimeric-DesAb-O (%)
Helix 1 (regular)	0.0	0.0
Helix 2 (distorted)	0.0	2.6
Anti-parallel 1 (left-twisted)	6.4	8.8
Anti-parallel 2 (relaxed)	34.7	29.9
Anti-parallel 3 (right-twisted)	15.5	21.9
Parallel	6.9	0.0
Turn	8.8	10.4
Others	27.7	26.3

Table 4.1 - Estimated secondary structure content (%) obtained with Best Sell software between the wavelength range of 195 and 250 nm. The total antiparallel β-sheet secondary structure was determined by summing all values relative to each type of antiparallel structure (left twisted, relaxed and right twisted), which was 56.6% for DesAb-O and 60.7% for the Dimeric-DesAb-O. The dimeric sdAb exhibits a 2.6% α-helix, likely attributable to the presence of the linker.

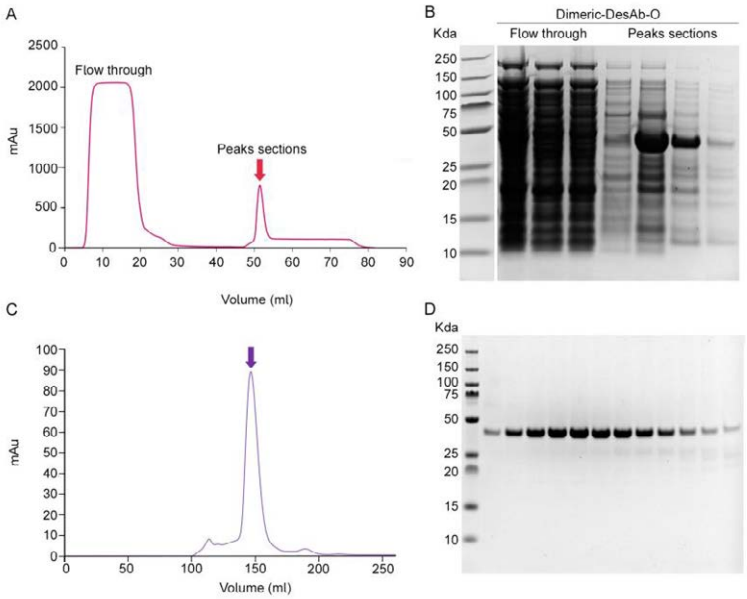

Figure 4.2 - Dimeric-DesAb-O expression and purification. A) Nickel-affinity chromatogram of the Dimeric-DesAb-O. Data were plotted using Excel (Version 16.89.1)

B) SDS-PAGE of samples taken after Nickel-affinity; flow through (lanes 1-3), peak sections (lane 4-7). The Dimeric-DesAb-O lane is indicated by the red arrow. C) SEC chromatogram of the Dimeric-DesAb-O. Data were plotted using Excel (Version 16.89.1). The peak relative to our protein is evidenced by the purple arrow. D) SDS-PAGE of Dimeric- DesAb-O peak sections taken after SEC to verify the sample purity.

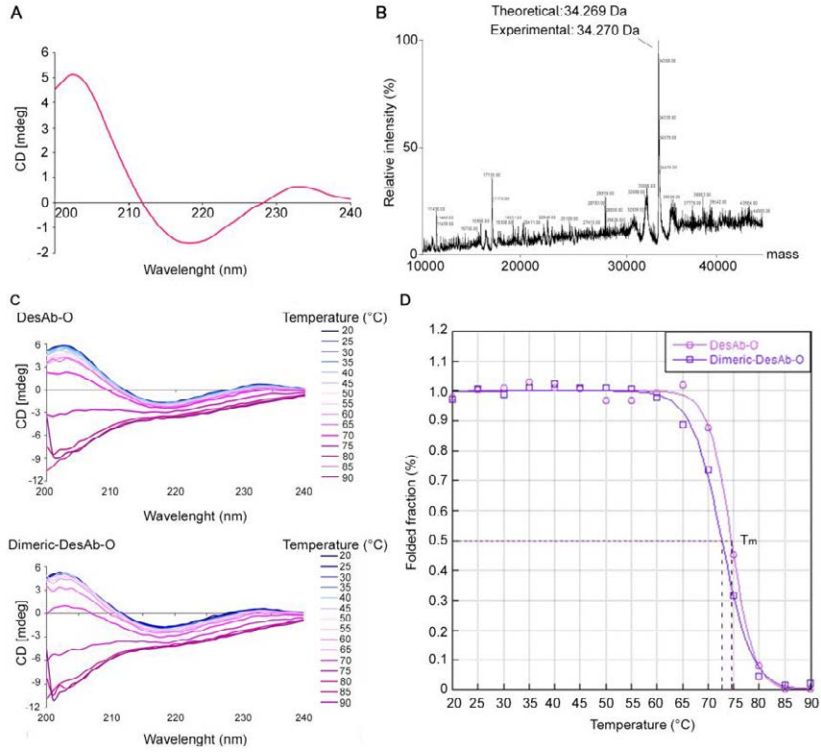

Figure 4.3 - Structural characterization of the Dimeric-DesAb-O. A) CD spectrum of the Dimeric- DesAb-O. The presence of peaks at 202 nm and 218 nm evidence the predominant β-sheet secondary structure of the dimeric sdAb. B) ESI-MS spectrum. Theoretical molecular weight was determined by ExPASy ProtParam software (34.269 Da) being perfectly in line with the mass observed by ESI-MS (34.270 Da). ESI-MS was performed by Lisa Haigh using the Chemistry Mass Spectrometry facilities available at the Molecular Sciences Research Hub, Department of Chemistry, Imperial College London. C) CD spectra of DesAb-O and the Dimeric-DesAb-O between 20 °C and 90 °C. D) DesAb-O and Dimeric- DesAb-O denaturation curves were obtained using the CD signal at 210 nm plotted against temperature, fitted with the Santoro and Bolen equation and normalized to fraction folded (%) values. Dimeric-DesAb- O had a temperature of half-denaturation (*Tm*) of 72.7 °C, while the value for DesAb-O was 74.6°C.

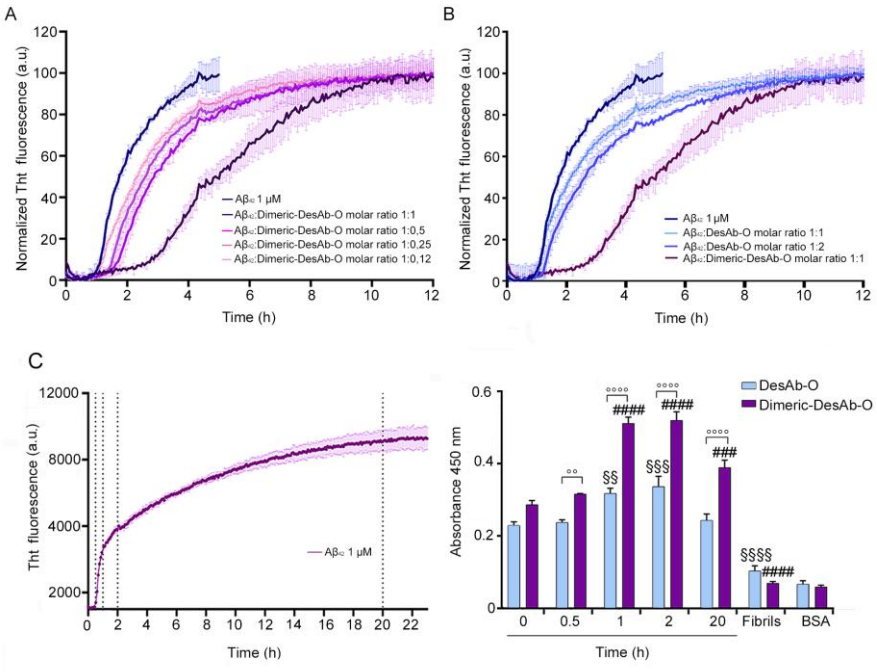

Figure 4.4 - The Dimeric-DesAb-O markedly interfere with $A\beta_{42}$ aggregation process and recognize with high specificity and sensitivity $A\beta_{42}$ oligomers. A) Representative ThT fluorescence assay of decreasing $A\beta_{42}$:Dimeric-DesAb-O molar ratios. 1 μM $A\beta_{42}$ (blue) was incubated with different Dimeric- DesAb-O molar ratios: 1:1 (dark purple), 1:0,5 (bright purple), 1:0,25 (dark pink) and 1:0,1 (pink). B) Representative ThT fluorescence assay of 1:1 $A\beta_{42}$:Dimeric-DesAb-O molar ratio and increasing $A\beta_{42}$:DesAb-O molar ratios as controls. 1 μM $A\beta_{42}$ (blue) was incubated with two DesAb-O molar ratios: 1:1 (bright light blue) and 1:2 (light blue). For the t_{50} quantification, we averaged three ThT aggregation assays. C) ThT-based *in vitro* aggregation assay of 1 μM Aβ42 (average of three replicates is shown). The black dashed lines indicate the time at which samples were collected from the aggregation reaction to perform the ELISA experiment. D) ELISA experiment performed on samples collected from the aggregation reaction shown in C, using DesAb-O and the Dimeric-DesAb-O as primary antibodies. $A\beta_{42}$ fibrils obtained after 4 days of incubation at 37 °C were used as a control. BSA signal represents the background absorbance values. The bar corresponding to DesAb-O is colored light blue while the one corresponding to the Dimeric-DesAb-O is purple. Error bars are representative of the S.E.M. Statistical analysis was performed by ANOVA with multiple comparison. Samples (n = 4) were analysed by Two-way ANOVA multiple comparison test comparing the absorbance of DesAb-O and Dimeric DesAb-O at the same times (°°P <0,01 and °°°°P<0,0001) and VS their respective time 0' (§§P <0,01, §§§P <0,005 and §§§§P<0,0001 for DesAb-O and ###P < 0,005, ####P < 0,0001 for Dimeric-DesAb-O).

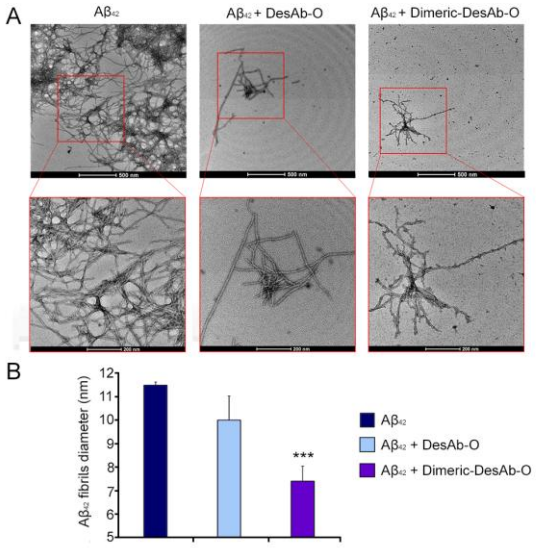

Figure 4.5 - $A\beta_{42}$ fibrils visualization and diameter quantification. A) TEM images of $A\beta_{42}$ fibrils obtained in the absence or in the presence of sdAbs at the end of a ThT aggregation assay. Higher magnifications of $A\beta_{42}$ fibrils are showed in the box area. B) $A\beta_{42}$ fibrils diameter quantification performed with ImageJ. Error bars are representative of the S.E.M (n = 3). For each TEM image, 15 to 25 diameter values were obtained and averaged. The mean value displayed in the graph represents the mean value of all the images for each condition. Measures were analysed by One-tailed t-test comparing the diameter width of the $A\beta_{42}$ fibrils obtained in the presence of the sdAbs VS the diameter width of the $A\beta_{42}$ fibrils obtained in absence of sdAbs (***P < 0,005 VS Dimeric-DesAb-O).

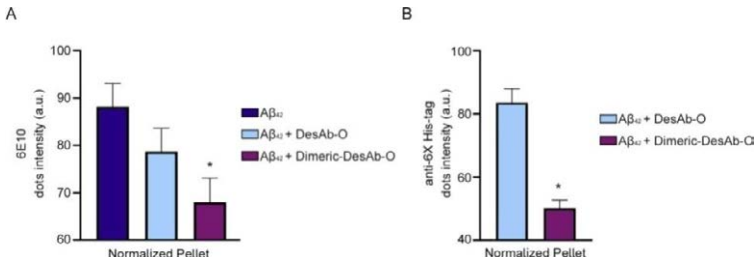

Figure 4.6 - Quantification of $A\beta_{42}$ fibrils and sdAbs deposited into the pellet. A) Pellet quantification of $A\beta_{42}$ fibrils obtained in the presence or absence of sdAbs normalized on total proteins signal. Error bars are representative of the S.E.M (n = 3). Samples were analyzed by One-Tailed Student t- test relative to Aβ fibrils obtained without antibody VS Aβ fibrils obtained in the presence of the Dimeric- DesAb-O (*P < 0.05) B) Pellet quantification of sdAbs deposited into the pellet normalized on total proteins signal. $A\beta_{42}$ signal was subtracted as background. Error bars are representative of the S.E.M (n = 2). Samples were analyzed by One-Tailed Student t-test to compare the presence of DesAb-O in the pellet compared to the Dimeric-DesAb-O (* P < 0.05)

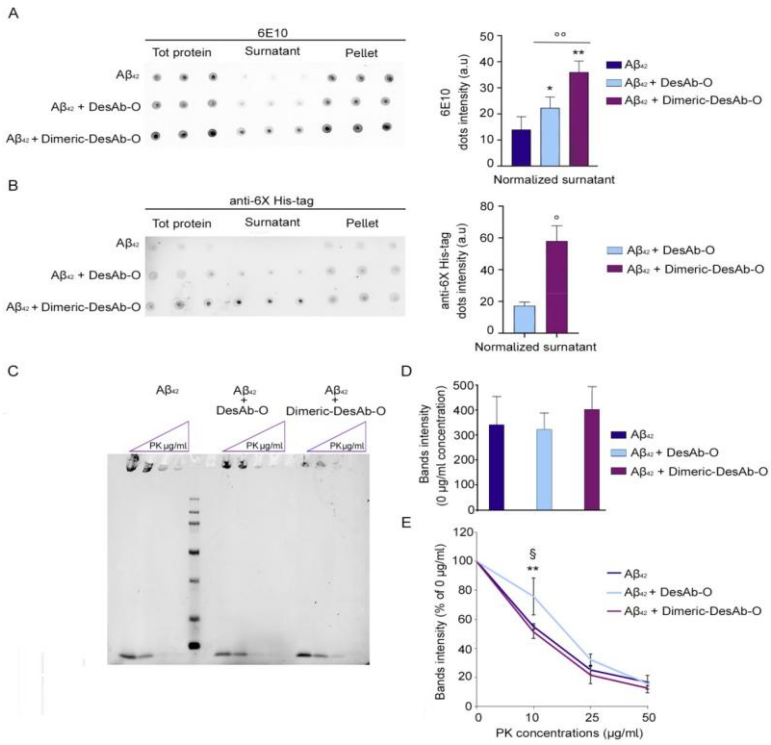

Figure 4.7 - Evaluation of $A\beta_{42}$ fibrils fragility and morphological changes induced by co-incubation with sdAbs. A,B) Dot Blot of total protein, surnatant and pellet of centrifuged Aβ42 fibrils samples obtained in co-incubation or not with sdAbs. The membranes were incubated with 6E10 (A) and anti-6X His-tag (B) as primary Abs for the quantification of $A\beta_{42}$ and sdAbs, respectively. $A\beta_{42}$ signal was subtracted as background. Error bars are representative of the S.E.M (n = 3 for 6E10 Ab and n = 2 for anti- 6X His-tag Ab). Samples were analyzed by One-Tailed Student t-test relative to $A\beta_{42}$ fibrils obtained without antibody VS $A\beta_{42}$ fibrils obtained in the presence of sdAbs (* $P < 0.05$ VS DesAb-O and ** $P < 0.01$ VS Dimeric-DesAb-O, respectively) or to $A\beta_{42}$ fibrils obtained in the presence of DesAb-O compared to $A\beta_{42}$ aggregates obtained in the presence of the Dimeric-DesAb-O (°° $P < 0.01$) or in panel B to compare the presence of DesAb-O in the supernatant compared to the Dimeric-DesAb-O (° $P < 0.05$). C) Representative Western Blot of $A\beta_{42}$ fibrils obtained in co-incubation with sdAbs or not treated with increasing PK concentrations (0, 10, 25, 50 μg/mL) for 30 mins. D) Quantification of 0 μg/mL bands intensity (n = 3) for each treatment. We can assess that all fibrils obtained in different conditions share a similar bands intensity at 0 μg/mL, demonstrating a consistent baseline across different treatment conditions, enabling reliable normalization of bands obtained at higher PK concentrations. E) Evaluation of $A\beta_{42}$ fibrils resistance to the PK digestion at increasing PK concentrations (0, 10, 25, 50 μg/mL). $A\beta_{42}$ fibrils obtained in the presence of DesAb-O showed a slightly increased resistance to the PK digestion at 10μg/mL. Experimental errors are S.E.M. (n = 3). Samples were analyzed by one-tailed Student t-test relative to Aβ fibrils obtained without antibody VS Aβ fibrils obtained in the presence of

DesAb-O (§ $P < 0.05$), or to Aβ fibrils obtained in the presence of Dimeric- DesAb-O compared to Aβ aggregates obtained in the presence of DesAb-O (** $P < 0.01$).

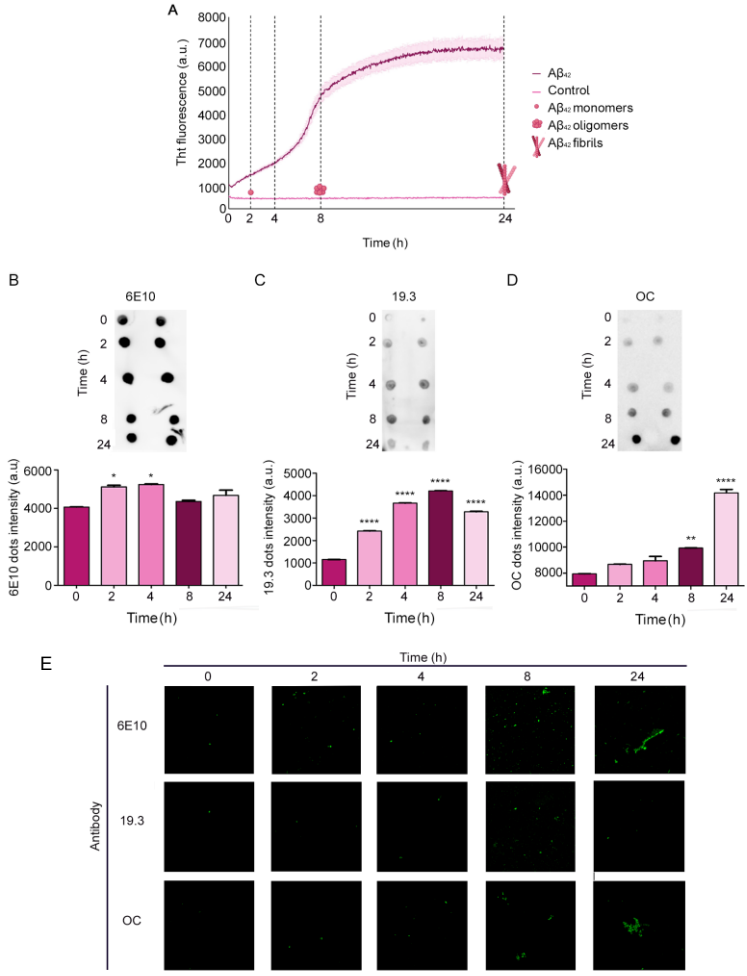

Figure 4.8 - Characterisation of $A\beta_{42}$ aggregates starting from the synthetic peptide. A) Monomeric $A\beta_{42}$ was incubated in PBS at 10 µM with 25 µM ThT dye. The plate was read in a BioTekSynergy^{TM}H1 Hybrid Multi-mode reader (Agilent, Santa Clara, United States) at 37 °C. Data were plotted using GraphPad Prism version 5.00 for Windows (GraphPad Software). Time points were collected at 0, 2, 4, 8 and 24 h to perform a characterization of $A\beta_{42}$ aggregates. B-D) Dot blot analysis and quantification of $A\beta_{42}$ samples collected at different timepoints. Samples of different $A\beta_{42}$ species were deposited (2 µl/spot) onto a nitrocellulose membrane and detected with the indicated antibodies (Abs). Membranes were incubated with 6E10 (B), 19.3 (C) and OC (D) primary Abs. The dot blot incubated with the 19.3 Ab showed the presence of oligomeric species since the early stage of the aggregation (2 h and 4 h) with the maximum amount reached at 8 h, consistent with the ThT assay showing the exponential phase at 8 h. From the dot blot obtained with the OC

Ab, we can see an increase of the dots intensity at 24 h, in line with the aggregation assay showing the reaching of the plateau due to the fibrils formation. Experimental errors are S.E.M. (n = 2). Samples were analysed by one-tailed Student t-test relative to their respective time 0 h (*P < 0,05, **P < 0.01, and ****P < 0.0001). E) STED microscopy images and visualisation of $A\beta_{42}$ samples collected at different timepoints. Samples of different $A\beta_{42}$ species were immunolabeled with 6E10, 19.3 and OC Abs. The STED microscopy images are perfectly in line with the dot blot assay results, showing the presence of oligomers since the initial stage of the aggregation $A\beta_{42}$ process as represented in 0, 2 and 4 h of 19.3 Abs images. After 24 h, the presence of fibrils is proved by the OC Abs signal confirming the aggregation assay and dot blot assay results.

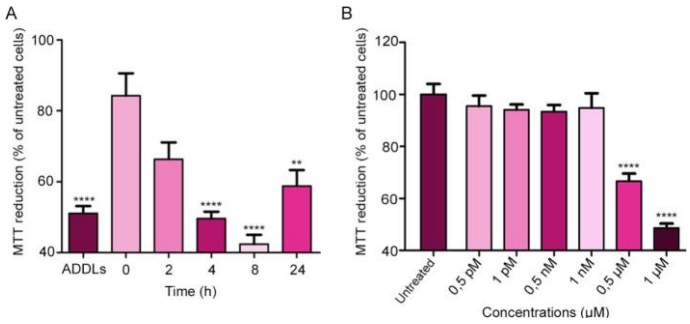

Figure 4.9 - $A\beta_{42}$ oligomeric species obtained after 8 h of incubation exhibit high toxicity. A) MTT reduction in SH-SY5Y cells treated for 24 h with various $A\beta_{42}$ aggregates (1 µM) obtained at different timepoints (0, 2, 4, 8 and 24 h) during aggregation (n = 2). ADDLs were used as a positive control. B) MTT reduction in SH-SY5Y cells treated for 24 h with $A\beta_{42}$ aggregates obtained after 8 h of aggregation in a dose-dependent manner. Experimental errors are S.E.M. (n = 3). Samples were analysed by One-way ANOVA followed by Bonferroni's multiple comparison test relative to untreated cells (**P<0.01 and ****P<0.0001).

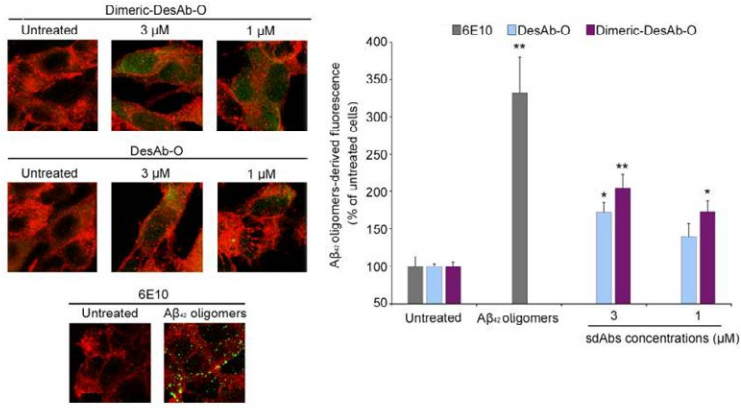

Figure 4.10 - The Dimeric-DesAb-O detects $A\beta_{42}$ oligomers interacting with neuronal cells at lower concentrations than DesAb-O. A) Representative confocal microscopy

images of SH-SY5Y cells treated with $A\beta_{42}$ species at 0.5μM for 1 h. Red and green fluorescence indicates respectively the cell membranes and the $A\beta_{42}$oligomers, detected respectively with wheat germ agglutinin (WGA) and sdAbs at two different concentrations of (3 μM or 1 μM). B) The histograms represent the results of a semi-quantitative analysis of the green fluorescent signal. Experimental errors are S.E.M. (n = 3). Samples were analyzed by one-tailed Student t-test to their respective untreated cells (*$P < 0.05$ and **$P < 0.01$). 200–250 cells were analyzed per condition.

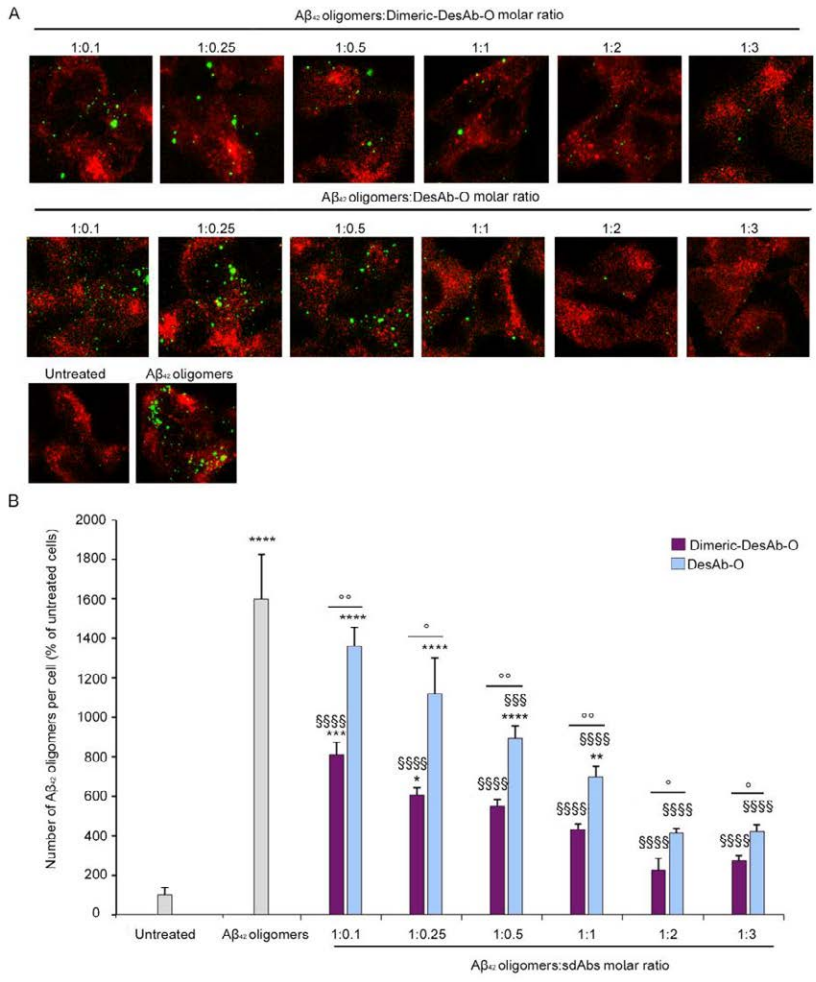

Figure 4.11 - The Dimeric-DesAb-O inhibits the binding of $A\beta_{42}$ oligomers to the neuronal membrane in a greater extent respect to DesAb-O. A) Representative confocal microscopy images of SH-SY5Y cells treated with 0.5 μM $A\beta_{42}$ oligomers following 1 h pre-incubation in the absence or in the presence of Dimeric-DesAb-O (first row) or DesAb-O (second row) at the indicated $A\beta_{42}$:sdAbs molar ratios. Red and green fluorescence indicates the cell membranes and $A\beta_{42}$ oligomers detected with WGA and 6E10 Ab, respectively. B) Count of $A\beta_{42}$ oligomers bound to the cellular membrane

measured following incubation under the conditions represented in panels A. Error bars indicate S.E.M. Statistical analysis was performed by ANOVA with multiple comparisons. Samples (n = 3) were analysed by one-way ANOVA followed by Bonferroni's multiple-comparison test to untreated cells (**$P < 0.05$, **$P < 0.01$, ***$P < 0.001$ and ****$P < 0.0001$), or to cells treated with $A\beta_{42}$ oligomers only (§§§§ $P < 0.001$ and §§§§ $P < 0.0001$) or to compare sdAbs at the same molar ratio (° $P < 0.05$ and °° $P < 0.01$).

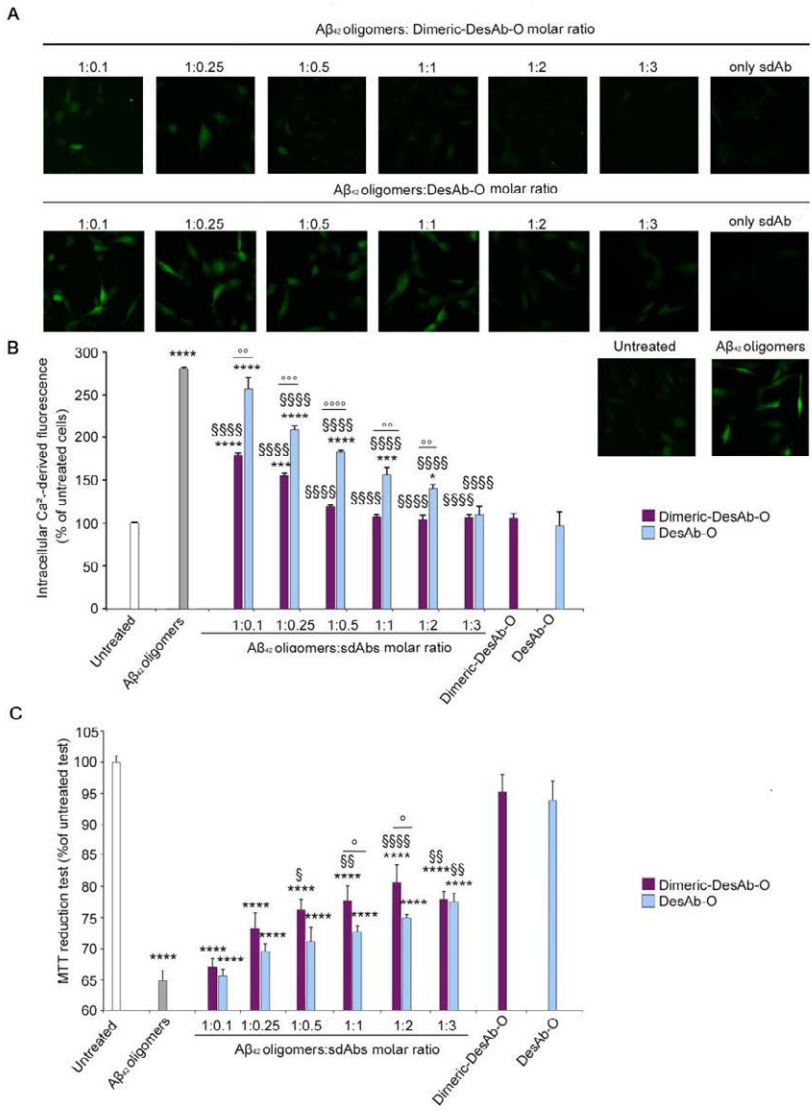

Figure 4.12 - The Dimeric-DesAb-O strongly prevents the neurotoxicity induced by $A\beta_{42}$ oligomers. A) Representative confocal microscopy images showing the Ca^{2+}- derived fluorescence in SH-SY5Y cells treated for 15 mins with 0.5 μM $A\beta_{42}$ oligomers with

increasing molar ratios (1:0.1, 1:0.25, 1:0.5, 1:1, 1:2, 1:3) of Dimeric-DesAb-O or DesAb-O. Cells were then loaded with the Fluo-4AM probe as described in the Methods section. B) Semi-quantitative analyses of the Ca^{2+}- derived fluorescence expressed as the percentage of the values for untreated cells. C) MTT reduction in SH-SY5Y cells treated for 24 h with increasing $A\beta_{42}$ oligomers:sdAbs molar ratios (1:0.1, 1:0.25, 1:0.5, 1:1, 1:2, 1:3). Errors are S.E.M. (n = 3 for confocal experiment and n = 4 for MTT). Samples were analyzed by One-way ANOVA followed by Bonferroni's multiple-comparison test to untreated cells (****P < 0.0001), or to cells treated with $A\beta_{42}$ oligomers (§ P < 0.05, §§ P < 0.01 and §§§§ P < 0.0001) or to compare sdAbs at the same molar ratio (° P < 0.05).

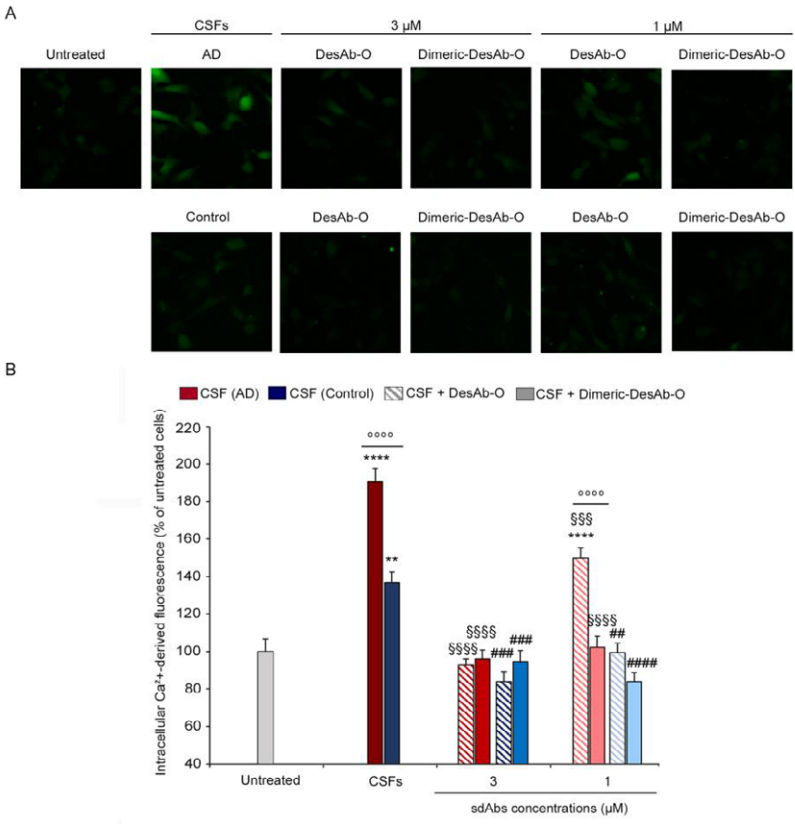

Figure 4.13 - The Dimeric-DesAb-O significantly reduce the Ca^{2+} dyshomeostasis induced by CSFs derived from AD patients. Intracellular Ca^{2+}-derived fluorescence in SH-SY5Y cells treated for 5 h with CSFs from AD patients and age-matched control subjects (n = 4), diluted 1:1 with the extracellular medium, following 1 h pre-incubation in the absence or in the presence of Dimeric-DesAb-O and DesAb-O at 3 µM or 1 µM. Experimental errors are S.E.M. Samples were analysed by One-way ANOVA relative to untreated cells (**P < 0.01 and ****P < 0.0001) or to cells treated with samples without DesAb-O (§§§ P < 0.001 and §§§§ P < 0.0001) or to compare the sdAbs at the same ratio (°°°° P < 0.0001).